Appl. Phys. A (2016) 122:795
DOI 10.1007/s00339-016-0343-x

Applied Physics A
Materials Science & Processing

Precise control of photoluminescence of silicon-vacancy color centers in homoepitaxial single-crystal diamond: evaluation of efficiency of Si doping from gas phase

Victor Ralchenko[1,2,3] · Vadim Sedov[2,3] · Vladimir Saraykin[4] · Andrey Bolshakov[2,3] · Evgeny Zavedeev[2,3] · Evgeny Ashkinazi[2,3] · Andrew Khomich[2,5]

Received: 9 May 2016 / Accepted: 4 August 2016 / Published online: 6 August 2016
© Springer-Verlag Berlin Heidelberg 2016

Abstract Ability to precisely control the Si-related color center abundance in diamond is important for the use of silicon-vacancy (SiV) defects with bright photoluminescence (PL) in quantum information technologies and optical biomarkers. Here, we evaluated the efficiency of Si incorporation in (100) plane of homoepitaxial diamond layers upon in situ doping by adding silane SiH_4 in the course of diamond chemical vapor deposition in microwave plasma using CH_4–H_2 mixtures. Both the Si concentration in the doped samples, as determined by secondary ion mass spectrometry, and PL intensity of SiV centers at 738 nm wavelength, measured at excitation wavelength of 473 nm, demonstrate a linear increase with silane content in feed gas in the range. The incorporation efficiency f, defined as the ratio of Si concentration in diamond to that in gas, $f = [Si/C]_{dia}/[Si/C]_{gas}$ is found to be $(1.1 \pm 0.5) \times 10^{-3}$ for the silane concentrations explored, $[SiH_4/CH_4] < 0.7$ %; thus, the Si atoms are accommodated in (100) diamond face easier than nitrogen and phosphorus, but more difficult than boron. This finding allows a tailoring of the Si content and photoluminescence intensity of SiV centers in in situ doped CVD diamond.

1 Introduction

Issues related to formation, properties and control of color centers in diamond are of vivid current interest due to promising applications of these photoluminescence (PL) sources such as single-photon emitters for quantum information technologies (QIT) operated at room temperature [1–5], optical biomarkers [6–8], sensors and monitors for synchrotron radiation beams [9, 10]. Silicon-vacancy (SiV) defect, comprising a silicon atom located between adjacent vacancies in the diamond lattice [11], has a strong and narrow zero-phonon line (ZPL) at 738 nm with a weak phonon sideband. More than 70 % energy is concentrated within ZPL [2, 5], thus making the photostable SiV center advantageous for QIT and other optical applications. Although the SiV center is easily formed, there is still a need to improve the methods for controllable doping of diamond with Si to be able to vary its concentration in a broad range.

Commonly, three main approaches are used to embed silicon atoms and obtain SiV centers: (1) The doping by Si^+ ion implantation provides a precise knowledge of the dose [12–14]; however, a residual damage may reduce the PL yield, and only a near-surface layer can be doped; (2) in situ doping in the course of diamond chemical vapor deposition (CVD) process, using Si-containing substrates like Si or SiO_2 [15–18], masks or standalone pieces of Si or SiC [19–22] or just a contamination on the CVD chamber walls, as a solid source of Si. The substrate is etched by atomic hydrogen of the plasma to form SiH_x radicals, participating further in the doping. However, this process is

✉ Vadim Sedov
sedovvadim@yandex.ru

1 Harbin Institute of Technology, 92 Xidazhi Str., 150001 Harbin, People's Republic of China

2 A.M. Prokhorov General Physics Institute RAS, Vavilov str. 38, Moscow, Russia 119991

3 National Research Nuclear University MEPhI, Kashirskoye sh. 31, Moscow, Russia 115409

4 Lukin Scientific Research Institute of Physical Problems, Zapadniy proyezd 5, Zelenograd, Moscow, Russia 124460

5 Institute of Radio Engineering and Electronics RAS, Vvedenskogo sq. 1, Fryazino, Russia 141190

not well controlled, since the amount of the Si precursor in the gas phase is not known; and (3) in situ doping using Si-containing gases, such as SiH_4 or $Si(OC_2H_5)_4$, as precursors [23–27]. This latter approach utilizing a gas-phase dopant precursor is routinely used for diamond doping with nitrogen, boron or phosphorous, for which the doping efficiency *f*, defined as the ratio between the particular impurity atoms in the gas phase and those into diamond, is well established [28–31]. However, this is not the case for diamond doping with silicon, for which the Si incorporation efficiency still is not known, and therefore, the precise doping control is problematic. To calculate the efficiency, the Si content in both gas and diamond must be determined. The Si impurity in diamond is typically measured by a secondary ion mass spectrometry (SIMS) [32–34]. In particular, using SIMS, Barjon et al. [32] found Si doping concentration up 3×10^{19} cm^{-3} in homoepitaxial diamond film by introducing a solid-state source of Si in CH_4-H_2 microwave plasma; however, they were unable to determine the doping efficiency *f* since the Si content in gas phase was principally unknown.

Here, we report on in situ doping of homoepitaxial single-crystal (SC) diamond layers with Si by adding silane SiH_4 into the microwave plasma to form SiV centers and study how the SiV PL emission can be precisely tuned by dosing the SiH_4. We found a clear correlation between SiV PL intensity, Si concentration in diamond and SiH_4 dopant in gas that allows a control of photoluminescent performance of the doped SC diamond. Finally, the incorporation efficiency of Si atoms in the diamond (100) plane has been evaluated. The epitaxial films of thickness in the range of 22–60 μm were produced by adding SiH_4 in CH_4–H_2 gas mixtures [25] in concentrations [SiH_4/CH_4] spanning from zero to 0.7 % to ensure the SiV PL intensity variations in a broad range (see *Experimental* section for further details). The case of even heavier doping, accompanied by a SiV PL emission quenching due to defects generation [25], is beyond the present study.

2 Experimental

The SC diamond films were deposited onto low-nitrogen, less than 100 ppb, (100)-oriented CVD diamond substrates of 2×2 mm^2 size in the MPCVD system ARDIS-100 (2.45 GHz) [25, 35] in 6 % CH_4/H_2 gas mixtures under the following process parameters: total gas flow of 500 sccm, gas pressure 130 Torr, microwave power 2.9 kW and substrate temperature 890 °C as measured by a two-color pyrometer (Willamson 81-35-C). The silane was added in the gas in concentrations [SiH_4/CH_4] varied from zero to 0.7 %. The epitaxial films of thickness in the range of 22–60 μm were produced with the growth rate of 15–17 μm/h.

The Raman and PL spectra, excited at 473 nm, were measured with a LabRam HR800 (Horiba Jobin-Yvon) spectrometer with the spectral resolution of 1.0 cm^{-1} and spatial resolution of ~1 μm. The laser beam was focused on the sample surface, and the light from the sample has been collected in backscattering geometry with the microscope objective (Olympus, magnification ×100, numerical aperture NA = 0.90). All the spectra were taken at room temperature at three different locations on the surface within a 1-mm zone in the sample's center and then were averaged. The PL SiV intensity I_{738} was normalized to the corresponding Raman diamond peak for each sample, to correctly compare the films with different thicknesses. It was checked that in the confocal configuration used, more than 90 % of the total PL signal comes from the top 20-μm-thick layer, typically less than the film thickness, so the contribution of the substrate to the spectra was insignificant [25].

The Si concentration in samples has been measured with secondary ion mass spectrometry (SIMS) using the IMS-4f instrument (Cameca) with mass resolution $m/\Delta m$ of 4000. The material sputtering was performed by O_2^+ primary ions with an energy of 8 keV, and the secondary ions $^{12}C^+$ and $^{28}Si^+$ were being analyzed. The etched area was 250×250 μm^2, while the SIMS signal was taken from 150×150 μm^2 in the crater center. For the SIMS signal calibration, ion implantation with $^{29}Si^+$ into growth side of a thick (0.5 mm) optical quality polycrystalline CVD diamond film (grain size ca. 100 μm) was performed at 200 keV energy and 2.5×10^{14} cm^{-2} dose. No PL signal from SiV has been detected in this calibration sample before the Si implantation.

3 Results and discussion

Figure 1 displays photoluminescence spectra for the Si-doped diamond films grown at different silane contents in gas. Each spectrum exited at 473 nm wavelength and taken in the wavelength region of 480–800 nm reveals only two features: the narrow Raman peak at 504 nm and a broader asymmetric band at 738 nm. The spectra were normalized to diamond Raman peak intensity to ensure that the PL signals, to be compared for different samples, refer to equal volumes of the crystals. The appearance of the strong peak at 738 nm for the doped epilayers is a result of SiV defect formation in the course of the CVD process, the PL emission intensity monotonically increasing with the SiH_4 content in gas. The SiV PL line position is found to vary slightly around the value of 738.5 ± 0.2 nm, while the line width (FWHM) ranges from 4.5 to 5.4 nm without any trend with the doping level. The observed variations in the 738 nm PL line width and position could be due to the

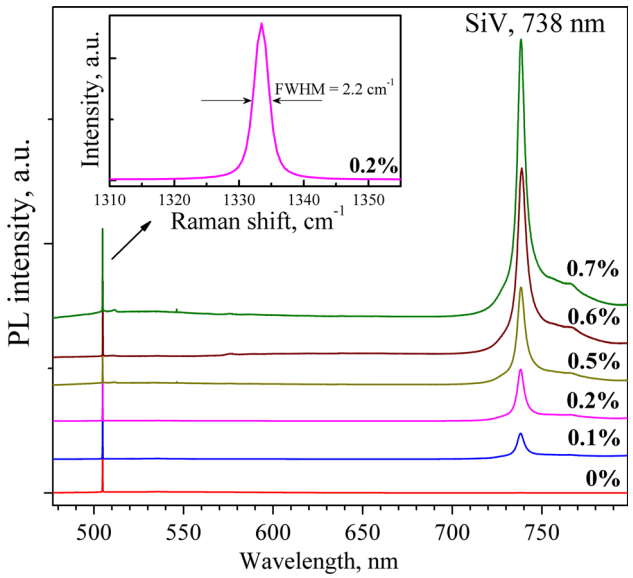

Fig. 1 PL spectra with SiV peak at 738 nm for Si-doped diamond films grown at different silane contents in gas (the percentage [SiH_4/CH_4] varied from zero to 0.7 % is indicated for each spectrum). The narrow line at 504.8 nm is diamond Raman peak. The spectra are exited at 473 nm wavelength, normalized to diamond Raman peak intensity and are displaced vertically for clarity. *Inset* high-resolution spectrum around diamond Raman peak

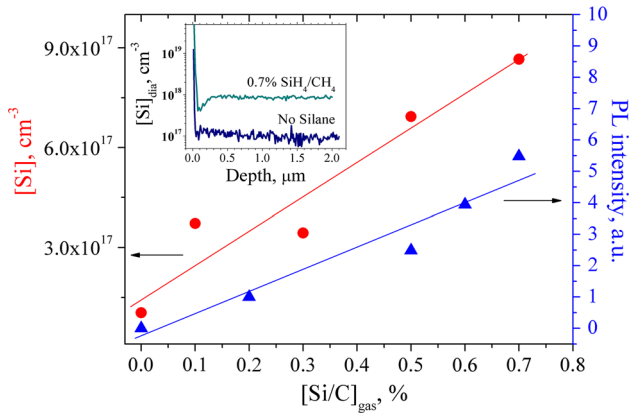

Fig. 2 Integrated SiV PL intensity (*triangles*) and concentration of silicon [Si] (*circles*) in Si-doped SC diamond films grown in SiH_4/CH_4/H_2 gas mixtures at different silane concentrations SiH_4/CH_4. The nominally undoped sample (0 % SiH_4/CH_4) shows a weak SiV PL as a result of contamination of the CVD system. The *straight lines* are least square fit for the experimental data. Inset: SIMS depth profiling of Si concentration for undoped and Si-doped ($SiH_4/CH_4 = 0.7$ %) films. The spikes in SIMS signal at small depth are due to surface contamination

presence of intrinsic stress in the films [36]. The 738 nm line intensity magnitude is comparable or larger than that for the Raman peak. The observed narrow Raman peak ($\Delta\nu = 2.2 \pm 0.2$ cm^{-1} FWHM) at 1332.5 ± 0.2 cm^{-1}, shown in inset in Fig. 1, characterizes low-defect diamond structure (we measured $\Delta\nu = 2.1$ cm^{-1} for a reference natural SC diamond). We note that the nominally undoped sample [SiH_4/CH_4]=0 % also revealed a SiV PL peak, although very weak (not seen within the scale in Fig. 1), as a result of the CVD system contamination with Si after previous deposition processes for silicon doping. However, the contribution of this additional, uncontrollable Si source to the PL emission of the doped films was less than 1 %.

The dependence of PL intensity I_{738} integrated over 700–800 nm wavelengths (area under the SiV peak) on silane concentration in the gas is shown in Fig. 2. The PL intensity increases linearly with the amount of silane added, following the increase in SiV centers content in the film, opening a deterministic way to control the SiV emission intensity by a proper choice of the growth/doping process parameters.

The Si atoms coupled to vacancies are known to constitute only a minor fraction of all Si impurity atoms introduced in diamond; there is, however, a serious discrepancy in the values of the [SiV]/[Si] ratio available in (quite limited) publications [25, 37]. To quantify the absolute concentrations [Si] in the samples, we measured it using a secondary ion mass spectrometry (SIMS) and a calibration sample of CVD diamond implanted with 200 keV $^{29}Si^+$ ions at known dose (see Experimental Section for further details). Examples of the SIMS depth profiling of Si concentration [Si] for undoped and Si-doped ($SiH_4/CH_4 = 0.7$ %) shown in Fig. 2 (see inset) demonstrate quite uniform doping through the entire depth of 2 μm. The plot for thus measured concentration [Si] versus silane content SiH_4/CH_4 in process gas is shown in Fig. 2 along with the PL intensity data. Again, the silicon content in diamond increases linearly with SiH_4 feed rate to reach $\approx 9 \times 10^{17}$ cm^{-3} (5 ppm) for the most doped film. The incorporation efficiency f, defined as the ratio of Si concentration in diamond to that in gas, $f = [Si/C]_{dia}/[Si/C]_{gas}$ is found to be equal to $(1.1 \pm 0.5) \times 10^{-3}$ for the doping parameters (SiH_4 concentrations) studied, as deduced from the slope of the SIMS data linear fit in Fig. 2.

It is instructive to compare the determined f value with those known for other important impurities such as N, B and P, commonly introduced in diamond and measured with nuclear reaction analysis (NRA), electron paramagnetic resonance (EPR) or SIMS. Such data, reported for (100)-oriented SC films grown by microwave plasma CVD [28–31], are summarized in Table 1. It follows that silicon incorporates in diamond easier than nitrogen and phosphorus ($f \approx 10^{-4}$), but more difficult than boron (10^{-1}–10^{-2}).

To examine how uniform laterally is the Si concentration over a sample area, a selected sample with dimensions of 4.2×3.7 mm^2 doped at [SiH_4/CH_4] = 0.6 % has been measured with SIMS at different locations along its 5.4 mm long diagonal, with interdistance of 0.8 mm

Table 1 Doping efficiency $f = [i/C]_{dia} / [i/C]_{gas}$ for some elements (i) incorporated in (100) SC diamond grown by MPCVD

Element	Precursor	f	Method
N	N_2	2×10^{-4}	NRA[28]
		$(0.75–1) \times 10^{-4}$	EPR[29]
		$(1.4–2.0) \times 10^{-4}$	NRA[30]
B	$C_3H_9BO_3$[a]	$10^{-1}–10^{-2}$	NRA[30]
P	PH_3	2×10^{-4}	SIMS[31]
Si	SiH_4	$(1.1 \pm 0.5) \times 10^{-3}$	SIMS[b]

[a] Trimethyl borate (TMB); [b]this work

between neighbor probed sites. Preliminarily, the sample has been mechanically polished to remove growth steps and achieve the surface roughness R_a below 2 nm on the main part of the (100) facet. The surface topography of the specimen, as measured with optical profilometer after the SIMS analysis (Fig. 3a), displays seven ≈600 nm deep pits with the size of 300 ≈ 300 μm^2 on the top surface narrowing to 200 ≈ 200 μm^2 on the bottom. As an example, the surface profile of a central pit is shown in Fig. 3b, and its bottom surface revealed very low surface roughness of $R_a = 1.3$ nm; thus, the ion beam-induced roughness was negligible and could not distort the obtained SIMS data. The Si concentration profile along the sample is shown in Fig. 3c. The Si distribution is quite uniform at the level of 5×10^{17} cm^{-3} within the central zone of ≈2.5 mm diameter, with significant, an order of magnitude, increase toward the sample edges, where macroscopic defects, such as polycrystalline inclusions, form.

To correlate the PL intensity with the Si content within this (100) facet, the SiV PL spectra were taken in the center of each pit etched upon the SIMS procedure and plotted in Fig. 3d. The PL profile closely mimics the [Si] profile, with a plateau in the central zone and an elevation toward the edges. The PL spectra were also taken outside each pit, in close proximity (~10 μm) to its border, with quite similar results, also displayed in Fig. 3d. We deduce from this comparison that: (1) Ion beam induces insignificant (if any) damage to the diamond surface in terms of the surface roughness modification and does not result in any degradation of SiV PL emission, and (2) SiV depth profile is quite uniform, at least across the top 500 nm, correlating with [Si] depth uniformity (see also inset in Fig. 2). The SiV concentration of ≈450 ppb for this particular sample has been determined from optical absorption spectrum [25], indicating that about 15 % of all silicon atoms are present in the form of SiV defect.

The enhanced PL emission is localized along the sample rim composed of polycrystalline diamond structure (Fig. 3c). The similar SiV PL enhancement effect on polycrystalline inclusions, of a few tens micrometer in size, has been recently reported by us for Si-doped epitaxial

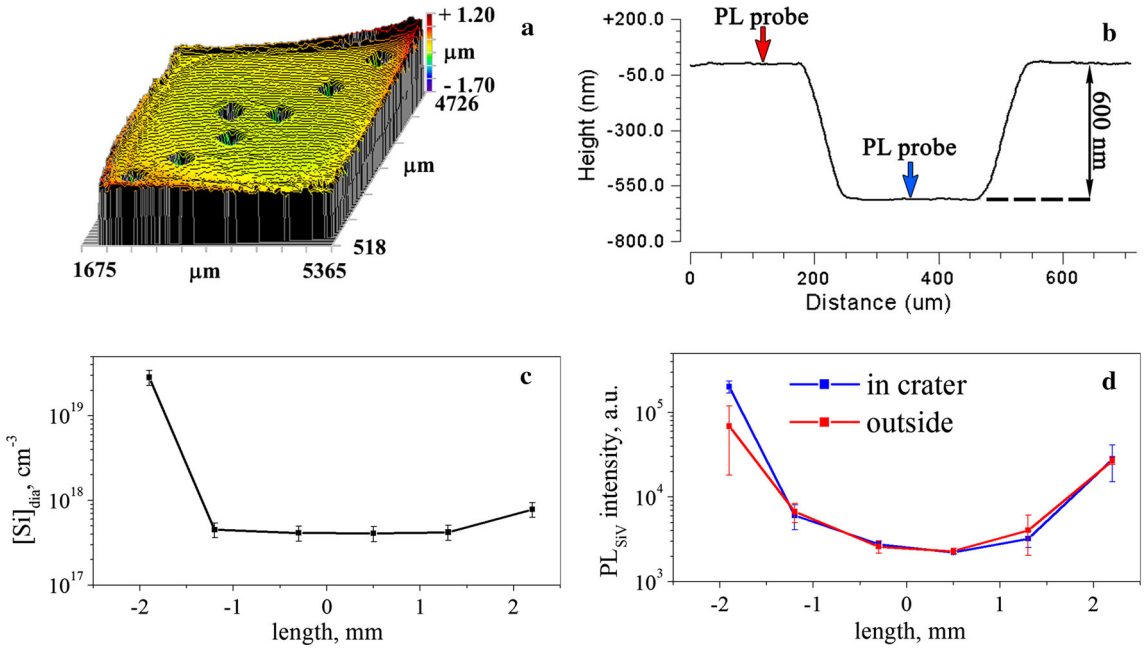

Fig. 3 **a** The map of pits etched in the course of SIMS measurements in epitaxial diamond film doped with Si with silane content $SiH_4/CH_4 = 0.6$ % in gas. The terminal pits at left and right sample's corners intercept, in a part, the polycrystalline rim on the sample edges. The image is taken with the optical profilometer. **b** The typical depth profile of the etched pit. **c** The Si concentration and **d** PL SiV integrated intensity in pits along the diagonal over the sample. The PL intensity has been measured inside the SIMS-produced pits (*blue squares*) and in 10 μm proximity but outside the crater (*red squares*)

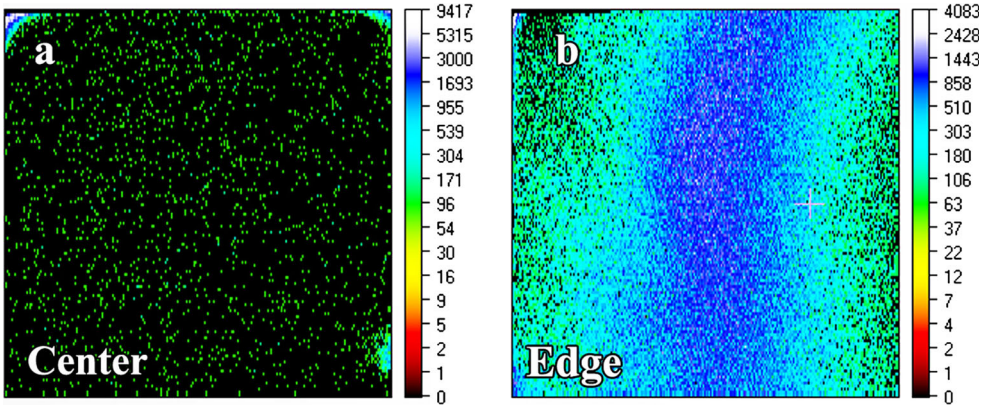

Fig. 4 The maps of SIMS signal for Si within the ion-etched craters in the central zone (**a**) and near the edge (**b**) of the sample. The area size is 200 × 200 μm

diamond films [25]. Several reasons for such PL enhancement on non-epitaxial inclusions were considered [25], including enhanced Si atoms incorporation in diamond due to tensile stress, appearance of ⟨111⟩ facets with better directionality of emitted photons and even a focusing of PL emission by the pyramidal-shaped defects; however, no clear explanation has been adopted, since the data on Si content in diamond were not available at that moment. It follows now from the profiles in Fig. 3c, d that the PL brightness increases in defected zone of *polished* surface simply owing to a higher Si concentration. To shed light on this issue, we analyzed here the Si spatial distribution *within* the craters in the course of SIMS measurement. The map of SIMS signal for Si within the ion-etched crater in the central part of the sample reveals a quite uniform Si distribution (Fig. 4a). In contrast, in the most distant crater, adjacent to the polycrystalline rim, the SIMS Si signal exhibits two zones with distinctly different Si abundance (Fig. 4b). This corroborates with the fact that a part of the crater crosses the edge-defected zone, which being enriched with Si shows the enhanced PL SiV emission. We conclude that the spatial variations in SiV PL emission over a diamond surface observed here and in the earlier work [25] reflect variations in Si concentration over the doped diamond film.

4 Conclusion

In summary, we demonstrated growth of homoepitaxial CVD diamond layers, in situ doped with Si by adding silane SiH_4, in variable concentration, in gas, and established a linear correlation between PL intensity of the formed SiV centers and Si concentration in diamond. The efficiency of incorporation of Si atoms into (100)-oriented diamond plane is determined quantitatively by SIMS and was found to be $(1.1 \pm 0.5) \times 10^{-3}$. This finding will allow a better control of the doping process with Si to obtain a desired content of SiV color centers to obtain a desired content of SiV color centers, which is important for photonic applications, including quantum optics, bio-labels and scintillators.

Acknowledgments This work was supported by the Russian Science Foundation, grant No. 14-22-00243.

References

1. S. Prawer, I. Aharonovich, *Quantum Information Processing with Diamond: Principles and Applications* (Elsevier, Amsterdam., 2014)
2. I. Aharonovich, E. Neu, Adv. Opt. Mater. **2**, 911 (2014)
3. F. Jelezko, J. Wrachtrup, Phys. Stat. Solidi (a) **203**, 3207 (2006)
4. I. Aharonovich, A.D. Greentree, S. Prawer, Nat. Photonics **5**, 397 (2011)
5. L.J. Rogers, K.D. Jahnke, T. Teraji, L. Marseglia, C. Müller, B. Naydenov, H. Schauffert, C. Kranz, J. Isoya, L.P. McGuinness et al., Nat. Commun. **5**, 4739 (2014)
6. L. Lai, A.S. Barnard, J. Nanosci. Nanotechnol. **15**, 989 (2015)
7. A.S. Barnard, I.I. Vlasov, V.G. Ralchenko, J. Mater. Chem. **19**, 360 (2009)
8. Y. Yoshinari, S. Mori, R. Igarashi, T. Sugi, H. Yokota, K. Ikeda, H. Sumiya, I. Mori, H. Tochio, Y. Harada et al., J. Nanosci. Nanotechnol. **15**, 1014 (2015)
9. R. Schirhagl, K. Chang, M. Loretz, C.L. Degen, Annu. Rev. Phys. Chem. **65**, 83 (2014)
10. M. Degenhardt, G. Aprigliano, H. Schulte-Schrepping, U. Hahn, H.J. Grabosch, E. Wörner, J. Phys: Conf. Ser. **425**, 192022 (2013)
11. J.P. Goss, R. Jones, S.J. Breuer, P.R. Briddon, S. Öberg, Phys. Rev. Lett. **77**, 3041 (1996)
12. C. Wang, C. Kurtsiefer, H. Weinfurter, B. Burchard, J. Phys. B: At. Mol. Opt. Phys. **39**, 37 (2005)
13. T.D. Merson, S. Castelletto, I. Aharonovich, A. Turbic, T.J. Kilpatrick, A.M. Turnley, Opt. Lett. **38**, 4170 (2013)
14. S. Tamura, G. Koike, A. Komatsubara, T. Teraji, S. Onoda, L.P. McGuinness, L. Rogers, B. Naydenov, E. Wu, L. Yan et al., Appl. Phys. Express **7**, 115201 (2014)
15. J. Riedrich-Möller, C. Arend, C. Pauly, F. Mücklich, M. Fischer, S. Gsell, M. Schreck, C. Becher, Nano Lett. **14**, 5281 (2014)
16. I.I. Vlasov, A.S. Barnard, V.G. Ralchenko, O.I. Lebedev, M.V. Kanzyuba, A.V. Saveliev, V.I. Konov, E. Goovaerts, Adv. Mater. **21**, 808 (2009)
17. E. Neu, C. Arend, E. Gross, F. Guldner, C. Hepp, D. Steinmetz, E. Zscherpel, S. Ghodbane, H. Sternschulte, D. Steinmueller-Nethl et al., Appl. Phys. Lett. **98**, 243107 (2011)

18. S. Singh, V. Thomas, D. Martyshkin, V. Kozlovskaya, E. Kharlampieva, S.A. Catledge, Nanotechnology **25**, 045302 (2014)
19. I. Aharonovich, J.C. Lee, A.P. Magyar, D.O. Bracher, E.L. Hu, Laser Photon. Rev. **7**, L61 (2013)
20. D. Sovyk, V. Ralchenko, M. Komlenok, A.A. Khomich, V. Shershulin, V. Vorobyov, I. Vlasov, V. Konov, A. Akimov, Appl. Phys. A **118**, 17 (2015)
21. V.S. Sedov, I.I. Vlasov, V.G. Ralchenko, A.A. Khomich, V.I. Konov, A.G. Fabbri, G. Conte, Bull. Lebedev Phys. Inst. **38**, 291 (2011)
22. A. Dietrich, K.D. Jahnke, J.M. Binder, T. Teraji, J. Isoya, L.J. Rogers, F. Jelezko, New J. Phys. **16**, 113019 (2014)
23. D.V. Musale, S.R. Sainkar, S.T. Kshirsagar, Diam. Relat. Mater. **11**, 75 (2002)
24. S.A. Grudinkin, N.A. Feoktistov, A.V. Medvedev, K.V. Bogdanov, A.V. Baranov, A.Y. Vul, V.G. Golubev, J. Phys. D Appl. Phys. **45**, 062001 (2012)
25. A. Bolshakov, V. Ralchenko, V. Sedov, A. Khomich, I. Vlasov, A. Khomich, N. Trofimov, V. Krivobok, S. Nikolaev, R. Khmelnitskii, V. Saraykin, Phys. Stat. Solidi (a) **212**, 2525 (2015)
26. V. Sedov, V. Ralchenko, A.A. Khomich, I. Vlasov, A. Vul, S. Savin, A. Goryachev, V. Konov, Diam. Relat. Mater. **56**, 23 (2015)
27. Y. Cui, J. Zhang, F. Sun, Z. Zhang, Trans. Nonferrous Met. Soc. China **23**, 2962 (2013)
28. R. Samlenski, C. Haug, R. Brenn, C. Wild, R. Locher, P. Koidl, Appl. Phys. Lett. **67**, 2798 (1995)
29. A. Tallaire, A.T. Collins, D. Charles, J. Achard, R. Sussmann, A. Gicquel, M.E. Newton, A.M. Edmonds, R.J. Cruddace, Diam. Relat. Mater. **15**, 1700 (2006)
30. R. Samlenski, C. Haug, R. Brenn, C. Wild, R. Locher, P. Koidl, Diam. Relat. Mater. **5**, 947 (1996)
31. H. Kato, S. Yamasaki, H. Okushi, Appl. Phys. Lett. **86**, 222111 (2005)
32. J. Barjon, E. Rzepka, F. Jomard, J.M. Laroche, D. Ballutaud, T. Kociniewski, J. Chevallier, Phys. Stat. Solidi (a) **202**, 2177 (2005)
33. I. Sakaguchi, M. Nishitani-Gamo, K.P. Loh, H. Haneda, S. Hishita, T. Ando, Appl. Phys. Lett. **71**, 629 (1997)
34. U.F.S. D'Haenens-Johansson, A.M. Edmonds, B.L. Green, M.E. Newton, G. Davies, P.M. Martineau, R.U.A. Khan, D.J. Twitchen, Phys. Rev. B **84**, 245208 (2011)
35. A.P. Bolshakov, V.G. Ralchenko, V.Y. Yurov, A.F. Popovich, I.A. Antonova, A.A. Khomich, E.E. Ashkinazi, S.G. Ryzhkov, A.V. Vlasov, A.V. Khomich, Diam. Relat. Mater. **62**, 49 (2016)
36. E. Neu, D. Steinmetz, J. Riedrich-Möller, S. Gsell, M. Fischer, M. Schreck, C. Becher, New J. Phys. **13**, 025012 (2011)
37. A.M. Edmonds, M.E. Newton, P.M. Martineau, D.J. Twitchen, S.D. Williams, Phys. Rev. B **77**, 245205 (2008)